Enhancement of Gas Sensitivity of Ferric Oxide Thin Films by Adding Activated Carbon Nanoparticles

R. M. T. D. RAJAPAKSHA[1], P. SAMARASEKARA[2], P. G. D. C. K. KARUNARATHNA[3], T. M. W. J. BANDARA[4], C. A. N. FERNANDO[5]

[1, 2, 4] *Department of Physics, University of Peradeniya, Peradeniya, Sri Lanka*

[3, 5] *Department of Nano Science Technology, Wayamba University of Sri Lanka, Kuliyapitiya, Sri Lanka*

Abstract- ***Thin films of ferric oxide (α-Fe_2O_3) were synthesized starting from iron acetate nano powder using the doctor blade method. Iron acetate powder was heated to 600 ^{0}C to crystallize the phase of ferric oxide. Then ferric oxide powder was mixed with PEG binder to make the thin film mechanically stable. Structural properties, grain size, strain and dislocation density of films were determined using the XRD patterns. Films with single phase of ferric oxide could be crystallized in thin film form according to XRD patterns. Chemical bonds in the thin films were investigated using FTIR spectrums. Optical band gap was measured using UV-Visible spectrums. Gas sensitivity was measured in 1000ppm of CO_2 gas by measuring the electric current using AUTOLAB. The optimum gas sensitivity could be obtained by adding 2% of activated carbon powder to α-Fe_2O_3 in mass ratio. Activated carbon added α-Fe_2O_3 thin film showed 50.2% sensitivity in 1000ppm CO_2 gas.***

I. INTRODUCTION

Due to the global air pollution, detecting the toxic gases received a vast attention recently. Iron oxide can be found in different phases such as magnetite, maghemite and hematite. Activated carbon finds potential applications in air purification, solvent recovery, decaffeination, methane and hydrogen storage, gold purification, metal extraction, water purification, medicine, sewage treatment, air filters, teeth whitening and production of hydrogen chloride. Semiconducting properties carbon-based carbon nanotube and activated carbon nanoparticles are important in many applications. Also, the higher effective surface area of carbon-based nanomaterials can absorb gases or radiation. Chemical and physical methods are applied to synthesize activated carbon nanoparticles. Activated carbon has been fabricated using plantain fruit stem [1]. Cedarwood and teak have been employed to prepare activated carbon [2]. Kenaf core fiber has been used to produce low cost activated carbon using acidic chemical activating agent [3]. Physical absorption of N_2 gas has been applied to measure the surface area kenaf core fiber activated carbon. Carbon based materials can be found in many applications as given below. Photovoltaic properties of dye sensitized solar cells have been improved using activated carbon TiO_2 composites based photoanode [4]. Activated carbon has been prepared using the oil fly ash in this study. Flexible and semi-transparent organic solar cells have been fabricated with different carbon-based materials such as carbon nanotubes and grapheme films synthesized by chemical vapor deposition [5]. Activated carbon is employed to design practical pressure swing thermal swing adsorption processes for separation and purification of gas mixtures [6]. Graphene anodes have been used to improve the performances of organic solar cells [7]. Highly flexible and stretchable carbon nanotube electrodes have been fabricated by simple brush painting for cost effective flexible organic solar cells [8]. However, activated carbon has not been applied to improve the gas sensitivity of ferric oxide by any researcher.

Iron oxide is a potential candidate of magnetic data storage, biosensing, drug delivery, magnetic resonant imaging and photodynamic therapy. Fe_2O_3 is a dark red material with band gap around 2.2 eV. The resistivity and activation energy of Fe_2O_3 at room temperature are $6.5x10^5$ Ωcm and 0.728eV, respectively. Fe_2O_3 thin film gas sensor sensitive to organic vapors and hydrogen gas have been synthesized using cathodic sputtering [9]. Fe_2O_3 gas sensing films have been deposited by normal pressure

chemical vapor deposition to detect acetone and alcohol [10]. Fe_2O_3 thick film sensors have been used to detect CH_4, H_2 and NH_3 [11]. Hollow balls of nano Fe_2O_3 has been employed to detect dimethyl methyl phosphonate at room temperature [12]. It is possible to control the gas sensing properties of hematite nanocrystals by controlling the morphology [13]. Gas sensing properties of p-type α–Fe_2O_3 polyhedral particles have been investigated [14]. Durability and stability of α–Fe_2O_3 oxide micro and nano structures have been studied [15].

Previously thin films have been synthesized using expensive techniques incorporated with vacuum by us [16-18]. Doctor blade method was found to be a low-cost deposition technique. Ferric oxide is a ferromagnetic material. For the first time, the addition of activated carbon nanoparticles to improve the gas sensitivity of ferric oxide is presented in this manuscript.

II. EXPERIMENTAL

Iron acetate powder was heated at 600 °C for 2 hours in a furnace. Then, 20 ml water was added to 0.15 g of polyethylene glycol (PEG) and, it was stirred for 15 minutes at 45 °C. Then 3 ml of prepared polyethylene glycol solution was added to the 1 g of iron oxide, and the solution was stirred for 2 hours at the room temperature to make pure iron oxide-PEG solution. Pieces of 3.5 cm×2 cm FTO glasses were used to fabricate the sample. Before depositing, an area of 1 cm×2 cm of the middle part of the conducting surface of the FTO glass was scratched in order to make that part non-conductive. Prior to the deposition, the FTO glasses were cleaned by sonicating in 10% (v/v) HCL in 30 minutes, and heated at 70 °C for 5 minutes in Acetone, Methanol and Isopropanol, respectively. Then the chemicals were washed out using distilled water. Finally, FTO glasses were dried using nitrogen gas. Thereafter, prepared solutions were fabricated on the conductive surface of the FTO glass using the doctor blade method. Finally, the samples were air dried for one hour and heated for 2 hours at 120 °C to remove excess air on the sample. Iron oxide was mixed with a suitable amount of activated carbon to make iron oxide-activated carbon solution. This solution was used to synthesize α–Fe_2O_3 films with activated carbon.

Thin films synthesized on scratched FTO glass substrates were used for the gas sensitivity measurements. The film was connected to 5 V power supply for 1 hour to stabilize the sensor. Then the sensing layer was connected to the gold coated electrodes in the gas chamber. The experimental setup was arranged by connecting the electrodes to a Keithley 6400 source meter AUTOLAB. The AUTOLAB instrument was in chronoampheometry measurement mode, and 5.0 V was applied. The current measurement time was set to 4000 s. After the setup reached a stabilized current level, CO_2 gas with 1000 ppm was injected in to the gas chamber. Then the current increased and stabilized at a maximum level. After the current was stabilized at the maximum level, normal air was injected to the gas chamber to remove the gas or vapor inside the chamber until the current stabilized at initial value. The same procedure was repeated for the doped and undoped samples.

Thin films fabricated on normal glass substrates were used for the X-ray Diffraction (XRD) analysis, UV-Visible spectroscopy, Fourier Transform Infrared (FTIR) spectrums and X-ray Fluorescence (XRF) spectrums. The structural properties of the thin films were determined by means of a X- Ray diffractometer Rigaku Ultima IV with Cu$K\alpha$ radiations. Optical band gap of the samples was measured using a Shimadzu 1800 UV-Visible spectrophotometer. Chemical bond types of the samples were investigated by a Shimadzu IR Affinity-1S at the wavenumber range of 400 cm^{-1} to 4500 cm^{-1}. Chemical compositions of the doped samples were found by means of a XRF analyzer. The impedance of samples was investigated using a Schlumberger SI 1260 impedance/gain phase analyzer.

III. RESULTS AND DISCUSSION

Figure 1 shows the XRD pattern of the samples with pure α–Fe_2O_3 (black curve) and α–Fe_2O_3 mixed with 2% activated carbon in mass ratio (red curve). Only the peaks of α–Fe_2O_3 appear in XRD pattern, and any peak of activated carbon is not observed. It can happen due to following reasons. Activated carbon can be in

amorphous phase. Or the trace amount of activated carbon does not produce XRD peaks with significant intensity. Or activated carbon is in the grain boundaries of α–Fe_2O_3 phase.

Crystallite size (D), dislocation density (δ) and strain (ε) of the samples were calculated using $D = \frac{0.91\lambda}{\beta\cos\theta}$, $\delta = \frac{1}{D^2}$ and $\varepsilon = \frac{\beta\cos\theta}{4}$, respectively. Where λ is the wavelength of Cu-Kα radiation (λ=1.54060 ^{0}A) and β is the full width at half maximum (FWHM) of XRD peak at angle θ. Values of the crystallite size, the dislocation density and the strain of pure α–Fe_2O_3 and 2% activated carbon mixed α–Fe_2O_3 films are given in table 1. Crystallite size slightly decreases due to the addition of activated carbon due to the additional grinding of powder. When the particle size decreases, the effective surface area required to absorb gas atoms increases. As a result, the gas sensitivity increases. However, the dislocation density and the strain increase due to the addition of activated carbon.

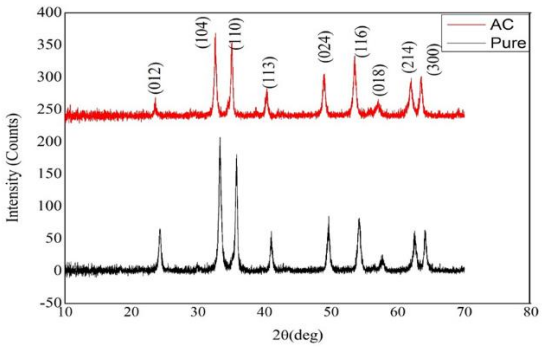

Figure 1: XRD patterns of pure and activated carbon added α-Fe_2O_3 thin films.

	angle 2θ (deg)	angle θ (deg)	FWHM (deg)	Crystallite size (10^{-7}m)	Dislocation density (10^{13} lines/ m^2)	Strain
Pure Fe_2O_3	35.039	17.52	0.246	1.37	5.33	0.0147
Activated Carbon 2% doped Fe_2O_3	35.026	17.51	0.310	1.12	8.02	0.0180

Table 1: The crystallite size, the dislocation density and the strain of pure α–Fe_2O_3 and activated carbon mixed α–Fe_2O_3 films.

Figure 2 shows the FTIR spectrum of activated carbon added α-Fe_2O_3 thin films. The spectrum indicates absorption at 3412, 1623, 1102, 544, and 452 cm^{-1}. The peaks at 452 and 544 cm^{-1} can be attributed to Fe-O stretching vibrational modes [31]. All the peaks belong to α-Fe_2O_3, and any peak related to bonding of activated carbon does not appear in the spectrum.

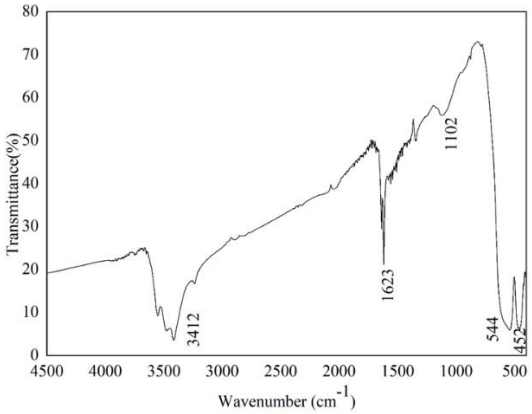

Figure 2: FTIR spectrums of activated carbon added α-Fe_2O_3 films.

Figure 3 shows the XRF of activated carbon doped α-Fe_2O_3 films. Here all the peaks belong to Fe.

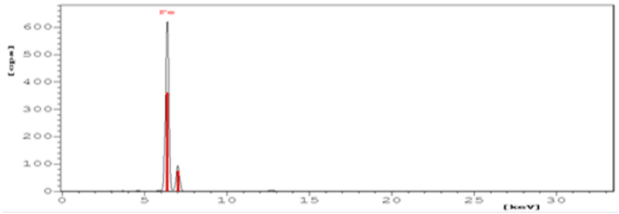

Figure 3: XRF of activated carbon doped α-Fe_2O_3 films.

Figure 4 shows the UV-Visible absorption spectrums of activated carbon doped α-Fe_2O_3 films. A tangential line was drawn to the absorption edge to calculate the optical band gap. The absorption edges of pure α-Fe_2O_3 and activated carbon added α-Fe_2O_3 films are 643.42 and 643.68 nm, respectively. Therefore, the optical band gaps of pure α-Fe_2O_3 and activated carbon added α-Fe_2O_3 films are 1.9319 and 1.9311, respectively. The optical band gap does not change due to addition of a small amount of activated carbon. This implies that the change of optical band gap is not attributed to the change of gas sensitivity. The enhancement of effective surface area of the sample due to the addition of activated carbon is attributed to the increase of gas sensitivity.

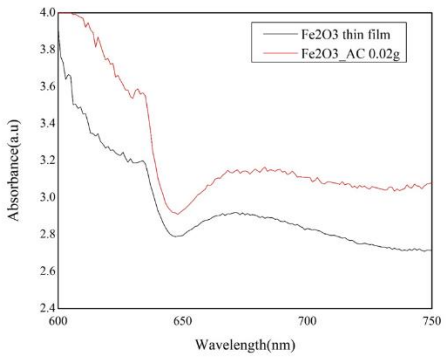

Figure 4: UV-Visible absorption spectrum of activated carbon doped α-Fe_2O_3 films.

Figure 5 shows the current and resistance versus time graphs for the 2% activated carbon added α-Fe_2O_3 thin films measured in 1000 ppm of CO_2 at the room temperature. The gas sensitivity, response time and recovery time of the pure α-Fe_2O_3 and the 2% activated carbon added α-Fe_2O_3 thin films calculated from graphs in figure 3 are presented in table 2. Activated carbon is a form of carbon processed to have small and low volume pores that increase the surface area available for adsorption or chemical reactions. Optimum amount of activated carbon that needs to enhance the gas sensing properties of α-Fe_2O_3 was found by preparing number of samples with different percentages of activated carbon. After adding 2% of activated carbon, the gas sensitivity of the α-Fe_2O_3 layer could be increased from 46% to 50.2%. However, the gas sensitivity could not be increased by adding more than 2% of activated carbon. The response time of activated carbon added sample is comparable to that of the pure α-Fe_2O_3 sample. The recovery time decreases due to the addition of activated carbon. By adding the activated carbon, the surface layer will act as an absorber and more analyte amount will be absorbed on the surface. Subsequently, they will react with oxygen bonds and release the electron in oxygen bonds. However, adding more activated carbon destroys the semiconducting surface of α-Fe_2O_3 and results in decreasing the gas sensitivity.

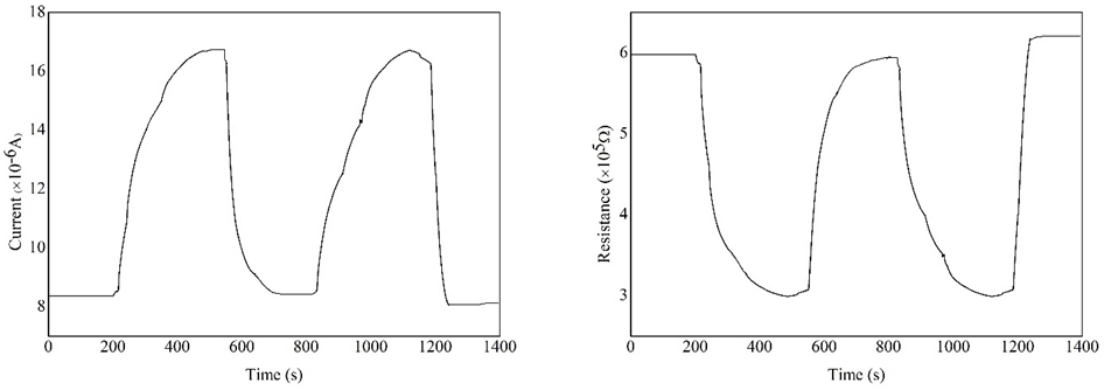

Figure 5: Current and resistance versus time graphs for activated carbon added α-Fe_2O_3 thin films

Doping Concentration	Response time(s)	Recovery time(s)	Gas Sensitivity %
Pure Fe_2O_3	300	400	46.0
AC added	294	318	50.2

Table 2: Gas sensitivity, response time and recovery time of pure α-Fe_2O_3 and 2% activated carbon added α-Fe_2O_3 thin films

Figure 6 shows the Nyquist plot of a pure α-Fe_2O_3 film. This graph is equivalent to Warburg impedance circuit. The linear part of the graph is related to the diffusion process. Electronic resistance of pure α-Fe_2O_3 film is almost zero. The charge transfer resistance of pure α-Fe_2O_3 film is 900 kΩ.

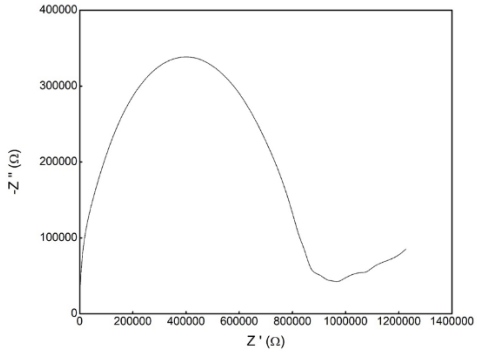

Figure 6: Nyquist plot of a pure α-Fe_2O_3 film

Figure 7 shows the Nyquist plot of an activated carbon doped α-Fe_2O_3 film. The electronic resistance of activated carbon doped α-Fe_2O_3 film is approximately 2 kΩ. The charge transfer resistance is about 80 kΩ. The charge transfer resistance drastically decreases due to the doping of activated carbon. The charge transfer resistance is related to the movement of electron from one atom to the other atom. This implies that activated carbon particles fill the voids of the sample and create a path for electron movement from one α-Fe_2O_3 atom to another atom.

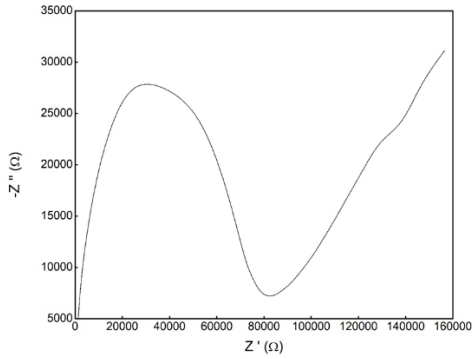

Figure 7: Nyquist plot of an activated carbon doped α-Fe_2O_3 film

CONCLUSION

According to the XRD patterns, addition of activated carbon does not change the Rhombohedral structure of α-Fe_2O_3. Adding activated carbon increases the effective surface area of the α-Fe_2O_3 sensing layer. As a result, the sample absorbs more gas atoms and does the sensing process more efficiently. The gas sensitivity could be increased up to 50.2% in 1000 ppm of CO_2 gas at the room temperature by adding the activated carbon nanoparticles. According to the impedance measurements, the charge transfer resistance decreases due to the addition of activated carbon nanoparticles. This indicates that the electrical conductivity of the sample enhances due to addition of the activated carbon. The enhancement of electrical conductivity is also attributed to the improvement of the gas sensitivity. However, adding more activated carbon results in decreasing the gas sensitivity because activated carbon reduces the gas absorption ability of the oxide surface. In addition, the decrease of particle size is attributed to the enhancement of the gas sensitivity FTIR images showed that any other metal bonds were not formed due to the doping. According to the UV-Visible spectrum, the optical band gap does not change due to the addition of activated carbon nanoparticle.

REFERENCES

[1] O.A. Ekpete, A.C. Marcus and V. Osi (2017). Preparation and characterization of activated carbon obtained from plantain (Musa Paradisiaca) fruit stem. Journal of Chemistry 2017, article ID 8635615.

[2] A.P. Ramirez, S. Giraldo, M. Ulloa, E. Florez and N.Y. Acelas (2017). Production and characterization of activated carbon from wood wastes. Journal of Physics: Institute of Physics conference series 935, article ID 012012.

[3] M.S. Shamsuddin, N,R,N, Yusoff and M.A. Sulaiman (2016). Synthesis and characterization of activated carbon produced from Kenaf core fiber using H3PO4 activation. Procedia Chemistry 19, 558.

[4] U. Mehmood, A.Z. Aslam, R.A. Shawabkeh, I.A. Hussein, W. Ahmad and A.G. Rana (2016). Improvement in photovoltaic performance of dye sensitized solar cell using activated carbon TiO_2 composites based photoanode. IEEE journal of photovoltaics 6(5), 1191.

[5] Z. Zhang, R Lv, Y. Jia, X. Gan, H. Zhu and F. Kang (2018). All-carbon electrodes for flexible solar cells. Applied Sciences 8, article ID 152.

[6] S. Sircar, T.C. Golden and M.B. Rao (1996). Activated carbon for gas separation and storage. Carbon 34(1), 1.

[7] Y. Wang, S.W. Tong, X.F. Xu, B. Ozyilmaz and K.P. Loh (2011). Interface engineering of layer-by-layer stacked graphene anodes for high performance organic solar cells. Advanced materials 23, 1514.

[8] D.Y. Cho, K. Eun, S.H. Choa and H.K. Kim (2014). Highly flexible and stretchable carbon nanotube network electrodes prepared by simple brush painting for cost effective flexible organic solar cells. Carbon 66, 530.

[9] Karel Siroky, Jana Jiresova and Lubomir Hudec (1994). Iron oxide thin film gas sensor. Thin Solid Films 245 (1-2), 211.

[10] J. Peng and C.C. Chai (1993). A study of the sensing characteristics of Fe_2O_3 gas sensing thin film. Sensors and Actuators B: Chemical 14 (1-3), 591.

[11] V.V. Malyshev, A.V. Eryshkin, E.A. Koltypin, A.E. Varfolomeev and A.A. Vasiliev (1994). Gas sensitivity of semiconductor Fe_2O_3 based thick-film sensors to CH_4, H_2, NH_3. Sensors and Actuators B: Chemical 19, 434.

[12] G. Fan, Y. Wang, M. Hu, Z. Luo, K. Zhang and G. Li (2012). Template free synthesis of hollow ball-like nano-Fe_2O_3 and its application to the detection of dimethyl methylphosphonate at room temperature. Sensors 12(4), 4594.

[13] Y. Yang. H. Ma, J. Zhuang and X. Wang (2011). Morphology controlled synthesis of hematite nanocrystals and their facet effects on gas sensing properties. Inorganic chemistry 50, 10143.

[14] N.V. Long, Y. Yang, M. Yuasa, C.M. Thi, Y. Cao, T. Nann and M. Nogami (2014). Gas sensing properties of p-type α–Fe_2O_3 polyhedral particles synthesized via a modified polyol method. RSC Adv 4, 8250.

[15] N.V. Long, Y. Yang, C.M. Thi, Y. Cao and M. Nogami (2014). Ultra-high stability and durability of α–Fe_2O_3 oxide micro- and nano structures with discovery of new 3D structural formation of grain and boundary. Colloids and Surfaces A: Physicochemical and Engineering Aspects 456, 184.

[16] P. Samarasekara (2009). Hydrogen and Methane Gas Sensors Synthesis of Multi-Walled Carbon Nanotubes. Chinese Journal of Physics 47(3), 361.

[17] H. Hegde, P. Samarasekara and F.J. Cadieu (1994). Nonepitaxial sputter synthesis of aligned strontium hexaferrites, $SrO.6(Fe_2O_3)$ films. Journal of Applied Physics 75(10), 6640.

[18] P. Samarasekara and F.J. Cadieu (2001). Polycrystalline Ni ferrite films deposited by RF sputtering techniques. Japanese Journal of Applied Physics 40, 3176.